American Journal of Engineering and Applied Sciences

Original Research Paper

A Classical Design Approach of Cascaded Controllers for a Traction Elevator

[1]Uko Victor Sorochi, [1]Kamalu Ugochukwu Anamelechi,
[1]Nwokocha Doris Adaugo and [2]Uko Ebenezer Ugochukwu

[1]*Department of Electrical/Electronic Engineering, University of Port Harcourt, Rivers State, Nigeria*
[2]*Department of Mechatronic Engineering, University of Port Harcourt, Rivers State, Nigeria*

Article history
Received: 13-07-2023
Revised: 25-07-2023
Accepted: 10-08-2023

Corresponding Author:
Uko Victor Sorochi
Department of
Electrical/Electronic Engineering,
University of Port Harcourt,
Rivers State, Nigeria
Email: victor_uko@uniport.edu.ng

Abstract: A traction elevator is a control system that can be driven by Direct Current (DC) motors. Premised on the reviewed literature, operations of control systems incorporated with DC motors are restrained by nonlinearities that deviate the controlled variables (position, speed, and torque) from the reference input. Controllers designed with appropriate gains annul the nonlinearities inhibiting the operation of a traction elevator. However, the literature did not account for detailed mathematical designs for the controller gains. Also, the modeled elevators had complex architectures. Hence, this research is aimed at modeling a simplified traction elevator and using the dynamics of its subsumes to mathematically design the gains of three controllers arranged in a cascaded topology to mitigate errors in the three control loops of the elevator. The Position of the elevator's car was controlled using a Proportional (P) controller while the Proportional-Integral (PI) controller controlled individually the speed and torque of the elevator's cabin. A novel objective function which was based on Integral Time Absolute Error (ITAE) was incorporated into the elevator's model to measure the deviation of the control variables from the input reference. The MATLAB Simulink environment was used in the modeling and simulation of the elevator system. The result obtained for the gain of the P controller for the elevator position, speed, and torque were 0.3652, 25.8, and 2.19, respectively. The gains of the integral controllers for the elevator speed and torque were 1372.3 and 219 respectively. A position reference of 100 m was used to verify the utilization of the controller gains. The result of the study improved existing literature because of the clarified elevator model and the output responses of the three controlled loops which were intuitive with lesser errors at steady state. For instance, steady-state errors of 3.54, 10.45, and 5% were obtained respectively in the position, speed, and current responses of the modeled elevator.

Keywords: Elevator, Controller, Cascade, MATLAB, Modelling, Simulation

Introduction

A vehicle that efficiently conveys passengers or cargo vertically (up or down) through building floors is called an elevator or a lift system. The elevators are becoming integral infrastructures in buildings because of the global population growth, blistering movement of people, and technological advancements in building architecture. Electric motors and pumped hydraulic fluids are two different types of prime movers that can be found in any elevator control system.

The subsumes of the traction elevator which are important to its functionality are the pulley drive, the counterweight, the motor, the power supply, the control system, the car, and the power converter. The car journeys up and down on guided vertical rails that are pendulous on a pulley system fitted on the motor shaft. Counterweights are also suspended on the pulley system to counterbalance the weight of the car. The electromechanical device called the electric motor functions as the driver of the traction elevator which can be powered by either an Alternating Current (AC) or a Direct Current (DC) source system. The control sub-block coordinates the operation of the elevator system (Daka, 2018).

There are two types of elevator systems which include hydraulic and traction elevators. The car of the hydraulic elevator is driven by electronic pumps which transmit hydraulics to the cylindrical jack or piston. The piston beneath the lift raises and lowers the elevator's car. The traction elevator was explored in this research work because its electric motor can be modeled mathematically. Furthermore, the traction elevator's system has a regenerative energy capacity and greater speed efficiency when likened to hydraulic elevators. Hence, making the traction elevators most commonly used in medium to high-rise buildings.

Contemporary passenger elevator designs that are widely used today were founded by Elisha Otis 1811-1861, a mechanic for a mattress firm in Yonkers, New York. Pebbles Kids Learning (2016). The traditional elevators were mired with intricate circuitries and complex wiring. This was because the elevators were controlled by relay-dependent controllers. These challenges can be ameliorated by automating the control circuitry of the elevator using the designed controllers in this research. For instance, in the research of (Yang *et al*., 2008) the elevator's controller was developed around a Programmable Logic Controller (PLC). Furthermore, (Sharkawy and Abdel-Jaber, 2022) presented a controller design for an elevator using a microcontroller called Arduino Uno.

Since the electric motor is the core driver of the traction elevator, special control measures were introduced to the DC motor that formed the hub of the traction elevator presented in this research work. The control measures aim at improving the performance of the DC motor which will invariably reduce errors in the entire elevator drive. The errors arise from the fact that process control systems making use of the DC motor are usually challenged by parameter variations, perturbations, and varying loads.

Peculiar insights were drawn from the research of (Khan *et al*., 2015) who utilized a Proportional Integral Derivative (PID) controller to control the speed of a DC motor under varying loads. Furthermore, (Adel *et al*., 2018) introduced a graphic user interface on MATLAB to visualize the behavior of a permanent magnet direct current motor. A microcontroller was used to control the speed of a DC motor in the research of (Vikhe *et al*., 2014). In another development, (Hummadi, 2012) controlled the speed of a DC motor using Linear Quadratic Regulator (LQR). Also, a vector-controlled scheme that utilized fuzzy logic was used to develop a controller for synchronous motors integrated into an elevator in the research of Yu *et al*. (2007). However, none of the literature was able to outline explicit design procedures for the parameters of the controllers used. Also, the modeled elevator had complex architectures void of a system for measuring errors in the control loops.

In this research, Proportional (P) and Proportional Integral (PI) controllers were deployed individually in a cascaded topology to control the position, speed, and torque of the elevator after detailed mathematical designs of the controllers' gains. The proportional controller for the position control was void of an integrator because it made position tracking sluggish. In a cascade topology, the set value of the first controller functions to control the set value of the next controller to mitigate errors in the system. The incorporated objective function in the elevator model of this research was used to measure errors in the controlled loops. "The advantages of cascade controller topology compared to single loop are flexibility, anti-jamming capability, and rapidity. Moreover, this control configuration reduces the time constant of the system." (Gücin *et al*., 2015). Furthermore, this research maximized two mechanical equations from the work (Daka, 2018) to simplify the architecture of the modeled elevator model.

Novelties of the Research in Summary

1. Mathematically obtained in detail, the gains of P and PI's controllers cascaded to mitigate errors retrogressing the control of the position, speed, and torque of a traction elevator
2. Modeled a simplified traction elevator on MATLAB and simulated it to visualize the improved responses with classically designed controllers
3. Successfully integrated an objective function to detect and measure the errors in the modeled elevator and to set the stage for the utilization of optimization algorithms to improve the overall control efficiency of the elevator

Materials and Methods

The methodology adopted in the research surpassed the referenced literature in that it was segmented into two. Firstly, mathematical representations of the elevator's subsumes were distinctly derived. Secondly, the mathematical representations were incorporated into respective MATLAB blocks (research materials) to model the elevator as shown in Fig. 11. Furthermore, the modeled elevator was simulated to obtain output responses for the individual control loops at various position references.

Mathematical Modelling of the Elevator's Three-Phase Full Wave Controlled Converter

The three-phase controlled rectifier of Fig. 1 was utilized in this research. This was because a higher DC output voltage was required which was higher than the voltage from a single-phase controlled rectifier.

The DC voltage (V_{dc}) that can be obtained from the rectifier of Fig. 1 was given by Eq. 1.

DOI: 10.3844/ajeassp.2023.92.105

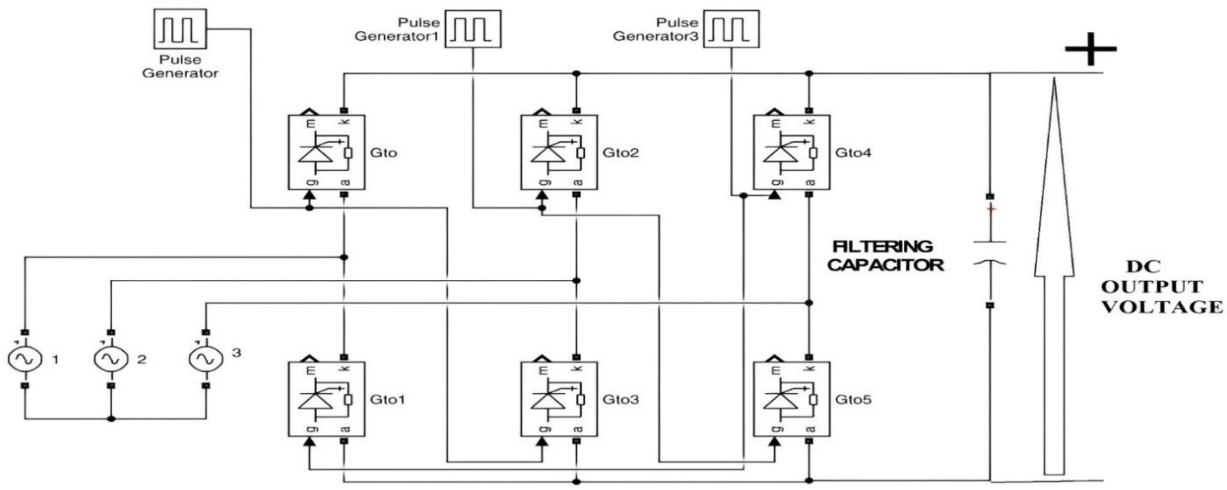

Fig. 1: A three-phase full wave-controlled rectifier

$$V_{dc} = \frac{3\sqrt{3}}{\pi} V_m cos \propto \tag{1}$$

where,
V_m = The peak value of the phase voltage (v)
$\propto$ = The firing angle of the thyristor

The maximum value of V_{dc} (*max*) was obtained when cos $\propto$ = 1. Hence Eq. 1 transforms to Eq. 2:

$$V_{dc} = (max) = \frac{3\sqrt{3}}{\pi} \tag{2}$$

The normalized control voltage (V_{cm}) of a single-phase controlled rectifier was given by Eq. 3:

$$V_{cn} = cos\alpha = \frac{V_c}{V_{cm}} \Rightarrow \propto = cos^{-1}\frac{V_c}{V_{cm}} \tag{3}$$

where,
V_c = The instantaneous control voltage
V_{cm} = The maximum limit of control voltage substituting Eq. 3 into Eq. 1:

$$V_{dc} = \frac{3\sqrt{3}}{\pi} V_m \frac{Vc}{V_{cm}} \tag{4}$$

where:

$$V_m = \sqrt{2} \times V_s \tag{5}$$

where,
V_s = The Root Mean Square (RMS) phase voltage
Substituting Eq. 5 into Eq. 4:

$$V_{dc} = 2.33 \times \frac{V_s}{V_{cm}} \times V_c$$

Let:

$$K_2 = 2.33 \times \frac{V_s}{V_{cm}}$$

The transfer function $G_r(S)$ of the three-phase full wave-controlled converter was given by Eq. 6:

$$G_r(s) = \frac{K_2}{1+ST_r} = \frac{2.33^{Vs} / V_{cm}}{1+ST_r} \tag{6}$$

where,
T_r = The converter time delay

Transfer Function Modelling of the Permanent Magnet DC Motor

The Fig. 2 represents the schematics of the permanent magnet DC motor that functions as the prime mover of the traction elevator utilized in the research. This section gave a detailed mathematical derivation for the DC motor model.

From the Fig. 2 since the field current i_f of the motor was kept constant (its source was from a constant DC supply) it implied that the induced e.m.f was proportional to the speed of the DC motor according to Eq. 7 in Laplace domain:

$$E_g \propto \omega_m \Rightarrow E_g(S) = K_b(S) \times \omega_m(S) \tag{7}$$

where,

E_g = The induced emf
K_b = A proportionality constant
ω_m = The speed of the DC motor

The armature voltage equation of the motor was obtained by taking KVL in the armature loop to obtain Eq. 8:

$$V_a = R_a I_a + L_a \frac{dI_a}{dt} + E_g \quad (8)$$

where,
R_a = Armature resistance
I = Current through the armature
L_a = Inductance of the armature coil

Equation 9 was obtained by taking the Laplace transform of Eq. 8:

$$V_a(S) = R_a I_a(S) + SL_a I_a(S) + E_g(S) \quad (9)$$

By simplifying Eq. 9 further, Eq. 10 was obtained:

$$I_a(S) = \frac{V_a(S) = E_g(S)}{R_a + SL_a} \quad (10)$$

The developed torque (T_d) of the dc motor relied on the current in the armature and field circuit according to Eq. 11:

$$T_d = K_t \times I_f \times I_a \quad (11)$$

where,
K_t = A constant of proportionality
I_f = The field's current
I_a = The armature current

Since I_f was kept constant, the product of K_t and I_f gave rise to a new constant K_b. Eq. 11 was then written as shown in Eq. 12:

$$T_d = K_b \times I_a \quad (12)$$

The mechanical equation which is the developed torque was given by Eq. 13:

$$T_d = J\frac{d\omega_m}{dt} + B_1\omega_m + T_L \quad (13)$$

where,
$J\frac{d\omega_m}{dt}$ = The Torque as a result of the inertia of the motor
ω_m = The speed of the DC motor
T_L = The torque developed as a result of the load connected to the machine
B_1 = The frictional coefficient of the DC motor

Taking the Laplace transform of Eqs.12-13 then Eqs.14-15 were obtained respectively:

$$T_d(S) = K_b \times I_a(S) \quad (14)$$

$$T_d(S) - T_L(S) = JS\omega_m(S) + B_1\omega_m(S) \quad (15)$$

Simplifying Eq. 15 will gave rise to Eq. 16:

$$\omega_m(S) = \frac{T_d(S) - T_L(S)}{B_1 + SJ} \quad (16)$$

The load attached to the shaft of the motor was modeled using Eq. 17:

$$T_L = B_L \times \omega_m \quad (17)$$

where,
B_L = The friction constant of the load

Taking the Laplace transform of Eq. 17 then Eq.18 was obtained:

$$T_L(S) = B_L(S) \times \omega_m(S) \quad (18)$$

Using Eq. 7, 10, 12, 14, 16, and 18 the control diagram of the DC motor was developed as shown in Fig. 3. The position control transfer function was obtained by placing an integrator at the output of the speed control loop.

The aim of the control diagram of Fig. 3. was to develop the DC motor transfer function and the respective transfer function equations for the current, speed, and position control loops using the block diagram reduction techniques. By using Eq.19, the load feedback loop in Fig. 3. was minimized to its equivalent Transfer Function (T.F) model:

$$T.F = \frac{G(S)}{1 + G(S)H(S)} \quad (19)$$

where:

$$H(S) = B_L \text{ and } G(S) = \frac{1}{B_1 + SJ}$$

$$T.F = \frac{1}{B_1 + SJ} \times \frac{B1 + SJ}{B_1 + SJ + B_L} = \frac{1}{B_1 + SJ + B_L}$$

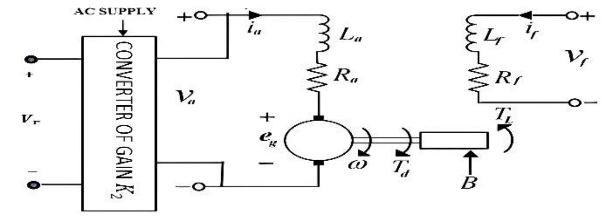

Fig. 2: Model of a separately excited DC motor

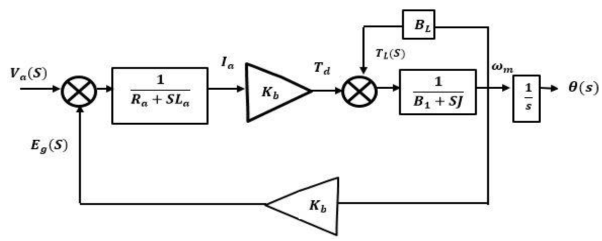

Fig. 3: Control diagram of a permanent magnet direct current motor

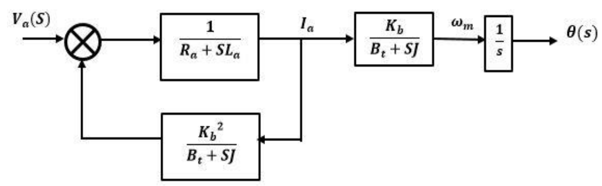

Fig. 4: Minimization effect of moving a take-off point

The sum of B_L and B_1 gave rise to B_t which was the total frictional constant. The control diagram of Fig. 3. was redrawn to what was shown in Fig. 4.

By applying Eq. 19 the feedback path of Fig. 4. was minimized:

$$G(S)=\frac{1}{R_a+SL_a}\ and\ H(S)=\frac{K_b^2}{Bt+SJ}$$

$$T.F=\frac{1}{R_a+SL_a}\times\frac{(Bt+SJ)(Ra+SLa)}{(Bt+SJ)(Ra+SLa)+K_b^2}$$

The transfer function of the DC motor was given by Eq. 20:

$$\frac{\omega_m(S)}{V_a(S)}=\frac{K_b}{(B_t+SJ)(R_a+SL_a)+K_b^2} \tag{20}$$

The transfer function relating the armature current I_a and voltage V_a was given by Eq. 21:

$$\frac{I_a(S)}{V_a(S)}=\frac{B_t+SJ}{(B_t+SJ)(R_a+SL_a)+K_b^2} \tag{21}$$

Simplifying Eq. 21:

$$\frac{I_a(S)}{V_a(S)}=\frac{Bt\left(1+\frac{SJ}{B_t}\right)}{R_aB_t+R_aJS+L_aB_tS+L_aJS^2+K_b^2}$$

Substitute:

$$\frac{J}{B_t}=T_m$$

where,

T_m = The time constant of the mechanical system. It is of the order of seconds
J = The machine inertia

$$\frac{I_a(S)}{V_a(S)}=\frac{B_t(1+sT_m)}{R_aB_t+R_aJS+L_aB_tS+L_aJS^2+K_b^2}$$
$$\frac{I_a(S)}{V_a(S)}=\frac{Bt}{K_b^2R_aB_t}\left(\frac{1+ST_m}{\frac{L_aJ}{K_b^2+R_aB_t}S^2+\frac{R_aJ+L_aB_t}{K_b^2+R_aB_t}S+1}\right) \tag{22}$$

By solving the quadratic equation of the denominator of Eq. 22 the roots (S_1 and S_2) were determined using the almighty equation:

$$(S_1,S_2)=\frac{-b\pm\sqrt{}\left(b^2-4ac\right)}{2a}$$

where:

$$a=\frac{L_aJ}{K_b^2+R_aB_t}\qquad b=\frac{R_aJ+L_aB_t}{K_b^2+R_aB_t}\qquad C=1$$

Substituting the variables of the almighty equation and simplifying will begat Eq. 23:

$$(S_1,S_2),=\left(\frac{1}{T_1},\frac{1}{T_2}\right)=-\frac{1}{2}\left(\frac{R_a}{L_a}+\frac{B_t}{J}\right)\pm\sqrt{}\left(\frac{1}{4}\right)\left(\left(\frac{R_a}{L_a}+\frac{B_t}{J}\right)^2-\frac{K_b^2+R_aB_t}{L_aJ}\right) \tag{23}$$

T_1 and T_2 were the poles of the current loop.

From Eq. 22 suppose:

$$K_1=\frac{B_t}{K_b^2R_aB_t}\ and\ (1+ST_1)(1+ST_1)=$$
$$\frac{L_aJ}{K_b^2+R_aB_t}S^2+\frac{R_aJ+L_aB_t}{K_b^2+R_aB_t}S+1$$

Bearing in mind that T_1 and T_2 are also called time constants which depended on the electrical and mechanical parameters of the DC motor.

The Eq. 22 was rewritten as shown in Eq. 24:

$$\frac{I_a(S)}{V_a(S)}=\frac{K_1(1+ST_m)}{(1+ST_1)(1+ST_1)} \tag{24}$$

DOI: 10.3844/ajeassp.2023.92.105

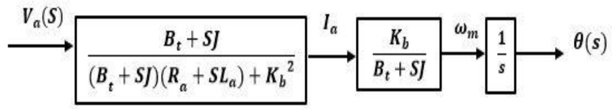

Fig. 5: Simplified control block for the DC motor

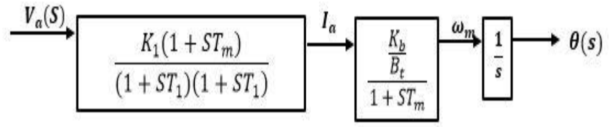

Fig. 6: Most simplified control block for the DC motor

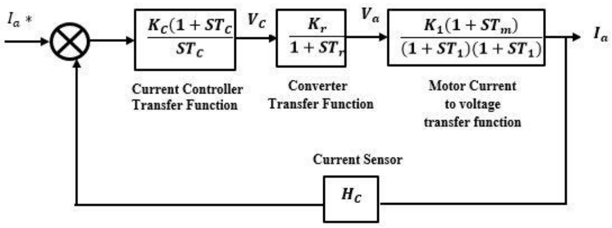

Fig. 7: Detailed current control loop

The block diagram of Fig. 5. was simplified based on the foregoing equation to yield Fig. 6.

The transfer function relating the speed of the motor ω_m and the armature current I_a from Fig. 6. was given by Eq. 25. It is also called the transfer function of the mechanical part of the motor:

$$\frac{\omega_m(S)}{I_a(S)} = \frac{K_b / B_t}{1+ST_m} \tag{25}$$

The transfer function relating the position of the motor $\theta(S)$ and the armature voltage V_a was given by Eq. 26:

$$\frac{\theta(S)}{Va(S)} = \frac{K_1 K_0 (1+St_m)}{B_t S(1+ST_1)(1+ST_1)(1+ST_m)} \tag{26}$$

Classical Design Approach for the Current Controller Gain

The current controller is the innermost loop and should possess the fastest response. Consider the structure of the current control loop of the DC motor shown in Fig. 7.

The open loop transfer function of Fig. 7. was gotten by multiplying the whole content of the block to give a fourth order transfer function equation. The fourth order arises from the four poles in the transfer function equation:

$$G(S)H(S) = \frac{K_C K_r K_1 H_C}{T_c} \times \frac{(1+ST_c)(1+ST_m)}{S(1+ST_1)(1+ST_2)(1+ST_r)} \tag{27}$$

where,
K_c = Gain of the current controller
K_r = Gain of the regulator
H_c = Current sensor gain
T_c = Current controller time constant
T_c = Motor time constant

The current loop equation was minimized with the help of a second-order equation via approximations.

Since the time constant of the mechanical system was smaller than that of the electrical system then:

$$(1+ST_m) \approx ST_m \tag{28}$$

Equation 27 was rewritten based on the approximation in Eq. 28:

$$G(S)H(S) = \frac{K_C K_r K_1 T_m}{T_c} \times \frac{(1+ST_c)}{(1+ST_1)(1+ST_2)(1+ST_r)} \tag{29}$$

Since $T_r < T_1 < T_2$ by setting $T_c = T_2$ the zero in the transfer function canceled one of the poles to give Eq. 30:

$$G(S)H(S) = \frac{K_C K_r K_1 T_m H_C}{T_c} \times \frac{1}{(1+ST_1)(1+ST_r)} \tag{30}$$

Let:

$$K = \frac{K_C K_r K_1 T_m H_C}{T_c} \tag{31}$$

where, K is the open loop gain of the current loop:

$$G(S)H(S) = \frac{K}{(1+ST_1)(1+ST\gamma)}$$

The characteristic equation was obtained from Eq. 31:

$$1 + G(S)H(S) = 0 \tag{32}$$

$$\begin{aligned} &1 + \frac{K}{(1+ST_1)(1+ST_r)} = 0 \\ &(1+ST_1)(1+ST_r) = K = 0 \\ &1 + ST_r + ST_1 + S^2 T_1 T_r + K = 0 \\ &S^2 + \frac{T_r + T_1}{T_1 T_r} S + \frac{1+K}{T_1 T_r} = 0 \end{aligned} \tag{33}$$

By comparing Eq. 32 with the general second-order system equation given by Eq. 34:

$$S^2 + 2\xi\omega_n S + \omega_n^2 = 0 \tag{34}$$

where,

ξ = Damping factor
ω_n = Natural frequency of the control system
ξ = selected as $\frac{1}{\sqrt{2}}$ in other to make the control system critically damped without overshoot:

$$\begin{gathered}\omega_n^2 = \frac{1+K}{T_1 T_r} \gg \omega_n = \sqrt{\left(\frac{1+K}{T_1 T_r}\right)} \\ 2\xi\omega_n = \frac{T_r = T_1}{T_1 T_r} \gg \xi = \left(\frac{\frac{\left(T_1 + T_r\right)^2}{T_1 T_r}}{(2)\sqrt{\left(\frac{K+1}{T_1 T_r}\right)}}\right) \\ K+1 = \left(\frac{\frac{\left(T_1 + T_r\right)^2}{T_1 T_r}}{\frac{2}{T_1 T_r}}\right)\end{gathered} \tag{35}$$

Suppose K >>1 and T_1>> T_r then $T_1+T_r \approx T_1$.
From Eq. 35:

$$K \approx \left(\frac{T_1^2}{2T_1 T_r}\right) \approx \frac{T_1}{2T_r}$$

Substituting the approximate value of K in Eq. 35:

$$\begin{gathered}\frac{T_1}{2T_r} = \frac{K_C K_r H_C K_1 T_M}{T_C} \\ K_C = \frac{1}{2}\left(\frac{T_1 T_C}{T_r}\right)\left(\frac{1}{K_1 K_r H_C T_m}\right)\end{gathered} \tag{36}$$

Equation 36 is the Gain of the current controller.

First Order Approximation of the Current Loop

In other to minimize the content of Fig. 7. the following assumptions were made. Suppose $T_c = T_2\ T_3+T_r$ and $1+ ST_m \approx ST_m$ (1 is ignored in the approximation because ST_m is very close to the gain cross-over frequency.) The Fig. 7. was minimized to obtain Fig. 8.

From Eq. 19 the closed loop transfer function of Fig. 8. can be represented by Eq. 37:

$$\frac{I_a(S)}{I_a *} = \frac{\frac{K_C}{T_C}\left(K_r K_1 T_m\right)\frac{1}{1+ST_3}}{\frac{1+K_1 K_C K_r H_C T_m}{1+\frac{K_1 K_C K_r H_C T_m}{T_C}\left(\frac{1}{1+ST_3}\right)}} \tag{37}$$

$$\frac{I_a(S)}{I_a *} = \frac{K_r K_C K_1 T_m}{T_C\left(1+ST_3\right)+K_1 K_r K_C H_C T_m} \tag{38}$$

Representing Eq. 38 with a first-order transfer function given in Eq. 39

$$\frac{I_a(S)}{I_a *} = \frac{K_i}{1+ST_i} \tag{39}$$

where,
K_i = The Gain of the current loop
T_i = The time constant of the current loop

Rearranging Eq. 38 to become the mirror image of Eq. 39 then Eq. 40 was obtained:

$$\frac{I_a(S)}{I_a *} = \frac{K_C K_r K_1 T_m H_c}{T_C} \times \frac{T_C}{H_C T_C\left(1+ST_3\right)+\frac{K_1 K_r K_C H_C T_m}{T_C}} \tag{40}$$

Suppose:

$$K_{fi} = \frac{K_C K_r K_1 T_m H_C}{T_C} \tag{41}$$

$$\frac{I_a(S)}{I_a *} = K_{fi} \times \frac{1}{H_C\left(1+ST_3\right)+K_{fi}}$$

$$\frac{I_a(S)}{I_a *} = \frac{K_{fi}}{H_C\left(1+K_{fi}\right)} \times \frac{1}{1+\left(\frac{ST_3}{1+K_{fi}}\right)} \tag{42}$$

Comparing Eq. 42 with Eq. 39 then Eqs. 43-44 were obtained:

$$K_i = \frac{K_{fi}}{H_C} \times \frac{1}{1+K_{fi}} \tag{43}$$

$$T_i = \frac{T_3}{1+K_{fi}} \tag{44}$$

Classical Design Approach for the Speed Controller Gain

The open loop transfer function equation of Fig. 9. was given by Eq. 45:

$$G(S)H(S) = \left(\frac{K_S K_i K_b K_w}{B_t T_S}\right) \times \left(\frac{1+ST_S}{S\left(1+ST_i\right)\left(1+ST_m\right)\left(1+ST_w\right)}\right) \tag{45}$$

Approximately, $1 + ST_m \approx ST_m$ and $T_w \times T_i \approx 0$.
Let:

$$T_4 = T_w + T_i$$

where,
T_w = The delay time of the speed loop
T_i = The delay time of the current loop

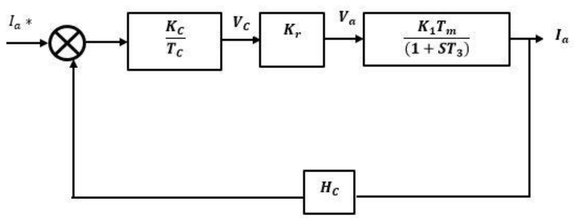

Fig. 8: First-order approximation of the current loop

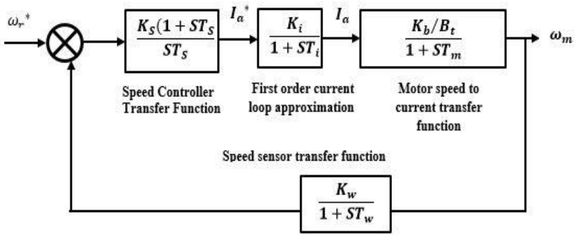

Fig. 9: Detailed Speed Control loop

Let:

$$G(S)H(S) = \left(\frac{K_S K_i K_b K_w}{B_t T_S T_m}\right) \times \left(\frac{1+ST_S}{S^2(1+ST_4)}\right)$$

$$K_2 = \frac{K_S K_i K_b K_w}{B_t T_S T_m}$$

$$G(S)H(S) = (K_2) \times \left(\frac{1+ST_S}{S^2(1+ST_4)}\right)$$

$$G(S)H(S) = \frac{K_2 K_S}{T_S} \times \frac{1+ST_S}{S^2(1+ST_4)}$$

Now, using Eq. 19 the closed loop transfer function of the speed loop was given by Eq. 46:

$$\frac{\omega_m}{\omega_m^*} = \frac{1}{K_w}\left(\frac{K_2 K_S / T_S\,(1+ST_S)}{S^3 T_4 + S_2 + SK_2 K_S + \frac{K_2 K_S}{T_S}}\right) \tag{46}$$

The transfer function of Eq. 46 was represented in generic form as given in Eq. 47:

$$\frac{\omega_m}{\omega_m *} = \frac{1}{K_w}\left(\frac{a_0 + a_1 S}{a_3 S^3 + a_2 S^2 + a_1 S + a_0}\right) \tag{47}$$

By comparing Eq. (46) with Eq. (47)

$$a_0 = \frac{K_2 K_S}{T_S} \qquad a_1 = K_2 K_S \qquad a_2 = 1 \qquad a_3 = T_4$$

$$\left|\frac{\omega_m}{\omega_m^*}\right| = \frac{1}{K_w}\sqrt{\left(\frac{a_0^2 + w^2 a_1^2}{a_0^2 + w^2\left(a_1^2 - 2a_0\right) + w^4\left(a_2^2 - 2a_1 a_3\right) + w^6 a_3^2}\right)}$$

To widen the bandwidth w^2 and w^4 terms are made zero:

$$a_1^2 = 2a_0 a_2 \gg K_2^2 K_S^2 = \frac{2K_2 K_S}{T_S} \gg T_S = \frac{2}{K_S K_2} \tag{48}$$

$$a_2^2 = 2a_1 a_3 \gg 1 = \frac{2K_2 K_S T_4}{T_S} \gg K_S = \frac{1}{2T_4 K_2} \tag{49}$$

Substitute the value of K_S (gain of the speed controller) of Eq. 49 into Eq. 48:

$$T_S = 4T_4 \tag{50}$$

Classical Design Approach for the Position Controller Gain

The position control loop transfer function was obtained by taking the integral of the DC motor speed control loop as shown in Fig. 10 to obtain Eq. 51:

$$\frac{\theta(S)}{\theta_{in}} = \frac{\left(\frac{1}{K_S}\right) \times \left(\frac{KK_b K_S}{R_a J}\right)}{\left(\frac{L_a}{R_a}S + 1\right)\left(S^2 + \left(\frac{R_a B_t + K_b}{R_a J}\right)S + \frac{KK_b K_S}{R_a J}\right)} \tag{51}$$

where,
K_S = The gain of the position sensor
K = The position controller gain

Since $\frac{L_a}{R_a} \approx 0$ Eq.51 was reduced to Eq. 52:

$$\frac{\theta(S)}{\theta_{in}} = \frac{\left(\frac{1}{K_S}\right) \times \left(\frac{KK_b K_S}{R_a J}\right)}{\left(S^2 + \left(\frac{R_a B_t + K_b}{R_a J}\right)S + \frac{KK_b K_S}{R_a J}\right)} \tag{52}$$

By comparing Eq. 52 with the general second-order system transfer function equation of Eq. 53:

$$T.F = \frac{W_n^2}{S^2 + 2\xi\omega_n S + \omega_n^2} \tag{53}$$

$$\frac{1}{K_S} = 1 \gg K_S = 1$$

$$2\xi\omega_n = \frac{R_a B_t + Kb^2}{R_a J} \tag{54}$$

$$\omega_n = \sqrt{\left(\frac{KK_b K_S}{R_a J}\right)} \tag{55}$$

Substituting Eq. 55 in 54 where $\xi = \frac{1}{\sqrt{2}}$

Table 1: Parameters of the DC motor used

Parameters	Rating
DC Motor rating	220V, 60H, 20A,
Motor-rated speed (N)	1570 rpm
Armature resistance of the motor (R_a)	6.5 Ω
Moment of inertia of motor (J)	0.060 kg-m^2
Armature inductance of motor	67mH
Viscus friction coefficient (B_t)	0.087 Nm/rad/sec
The maximum control voltage of the rectifier (V_{cm})	±10v
Line-to-line AC voltage to the converter	230v
Current $I_{max\ was}$ taken in by the DC motor	20A
Torque constant (K_b)	1.24 rad/sec
Speed Sensor transfer function	$G(S)=\frac{0.065}{1+0.002S}$
Rated power of machine (watts)	4400

$$\frac{2}{\sqrt{2}}\times\sqrt{\left(\frac{KK_bK_S}{R_a}\right)}=\frac{R_aB_t+K_b^2}{R_aJ}$$

$$K=\frac{R_aJ}{2K_bK_S}\sqrt{\left(\frac{R_aB_t+K_b^2}{R_aJ}\right)} \quad (56)$$

Equation 56 is the gain of the position controller.

Numerical Substitution for the DC Motor Drive Equations

The numerical substitutions in this section were achieved by utilizing the necessary parameters from Table 1 Phase voltage:

$$(V_S)=\frac{V_L}{\sqrt{3}}$$

where,

V_L = The line-to-line voltage of the AC source fed to the converter:

$$(V_S)=\frac{V_L}{\sqrt{3}}=\frac{230}{\sqrt{3}}=127.02v$$

$$K_2=2.339\times\frac{V_S}{V_{cm}}=2.339\times\frac{127.02}{10}=29.71$$

$$V_{dc}(max)=K_2\times V_c$$

(Here at maximum values, $V_c = Vc_m$):

$$V_{dc}(max)=29.71\times10=297.10v$$

The control voltage V_c at which the rated 220v of the motor was obtained is given by:

$$V_c\ \frac{V_{dc}}{V_{dc}(max)}\times V_{cm}=\frac{220}{297.10}\times10=7.41v$$

Converter time delay:

$$T_r\ \frac{1}{12f}=\frac{1}{12\times60}=0.00138sec$$

From Eq. 6 $G_r(S)=\frac{K_r}{1+ST_r}=\frac{29.71}{1+0.00138sec}$.

$$H_C=\frac{Maximum\ control\ voltage\ for\ the\ rated\ voltage}{maximum\ current\ drawn\ by\ the\ motor\ from\ supply}$$

$$=\frac{7.41}{20}=0.3705v/A$$

By substituting the value of the variables in Eq.23 from Table 1 and simplifying:

$$S_1=-5.64\gg T_1=0.18 \quad \text{and} \quad S_2=-92.83\gg T_2=0.01\ sec$$

Mechanical time constant:

$$T_m=\frac{J}{B_t}=\frac{0.06}{0.087}=0.69sec$$

$$K_1=\frac{B_t}{K_b^2R_aB_t}=\frac{0.087}{(1.24^2)+(6.5)(0.087)}=0.0404$$

$$\frac{I_a(S)}{V_a(S)}=\frac{K_1(1+ST_m)}{(1+ST_1)(1+ST_1)}=\frac{0.0414(1+0.069S)}{(1+0.18S)(1+0.01S)}$$

$$\frac{\omega_m(S)}{I_a(S)}=\frac{14.253}{1+0.69S}$$

$$\frac{\omega_m(S)}{V_a(S)}=\frac{1.24}{(0.087+0.06S)(6.5+0.067S)+1.5376}$$

$$T_C=T_2=0.01sec$$

From Eq. 36:

Table 2: Mechanical parameters of the elevator (Daka, 2018)

Parameters	Ratings
The radius of the elevator's car pulley (R)	0.0955 m
Pulley inertia (J_P)	0.1kg. m^2
Motor frictional coefficient (b_m)	0.0869 N.m.s
Motor Inertia (J_m)	0.05 kg. m^2
Gravitational acceleration (g)	9.81 m/s^2
Maximum elevator car load	390 kg
Mass of the elevator's car	100 kg
Counter mass (M_{cw})	300 kg

$$K_C = \frac{1}{2}\times\frac{(0.18)(0.01)}{(0.00138)}\times\frac{1}{0.0414\times 29.71\times 0.37025\times 0.69} = 2.19$$

The transfer function of the current controller:

$$\frac{K_C(1+ST_C)}{ST_C} = \frac{2.19(1+0.01S)}{0.01S} \tag{57}$$

By comparing Eq. 57 with the general transfer function equation of the PI controller given in Eq. 58:

$$\frac{E_a(S)}{E(S)} = \left(K_P + \frac{K_1}{S}\right) \tag{58}$$

where, K_p is the gain of the proportional controller and K_I is the gain of the integral controller:

$$K_{p\,current} = 2.19 \qquad K_{I\,current} = 219$$

$$K_{fi} = \frac{K_C K_r K_1 H_C}{T_C} = \frac{(2.19)(29.7)(0.0414)(0.69)(0.3705)}{0.01} = 68.77$$

From Eq. 43:

$$K_i = \frac{K_{fi}}{H_C}\times\frac{1}{1+K_{fi}} = \frac{68.77}{0.3705}\times\frac{1}{1+68.77} = 2.66$$

$$T_3 = T_1 + T_r = 0.18 + 0.00138 = 0.18138\,sec$$

$$T_i = \frac{T_3}{1+K_{fi}} = \frac{0.00138}{1+68.77} = 0.0026\,sec$$

Substituting the values of the variables in Eq. 38:

$$\frac{I_a(S)}{I_a{*}(S)} = \frac{K_i}{1+ST_i} = \frac{2.66}{1+0.0026S}$$

$$T_4 = T_i + T_W = 0.0026 + 0.00216 = 4.76\,ms$$

$$K_2 = \frac{K_S K_i K_b K_w}{B_t T_S T_m} = \frac{1\times 2.66\times 1.24\times 0.0741}{0.087\times 0.69} = 4.0715$$

$$K_S = \frac{1}{2K_2T_4} = \frac{1}{2\times 4.0715\times 4.76\times 0.001} = 25.8$$

$$T_S = 4\times T_4 = 4\times 4.76\,ms = 0.0188\,S$$

Speed controller transfer function:

$$K_S\frac{1+ST_S}{ST_S} = 25.8\frac{(1+0.0188S)}{0.0188S} \tag{59}$$

Comparing Eq. 59 with Eq. 58

$$K_{p\,speed} = 25.8 \qquad K_{I\,speed} = 1372.3$$

From Eq. 56:

$$K_{p\,position} = \frac{R_a J}{2K_b K_S}\sqrt{\left(\frac{R_a B_t + K_b^2}{R_a J}\right)} = \frac{6.5\times 0.06}{2\times 1.24\times 1}\times\left(\sqrt{\frac{(6.5\times 0.087)+(1.24^2)}{6.5\times 0.06}}\right)$$

$$K_{p\,position} = 0.15726\times 2.322 = 0.3652$$

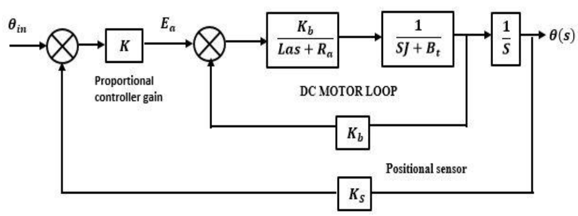

Fig. 10: Detailed position control loop

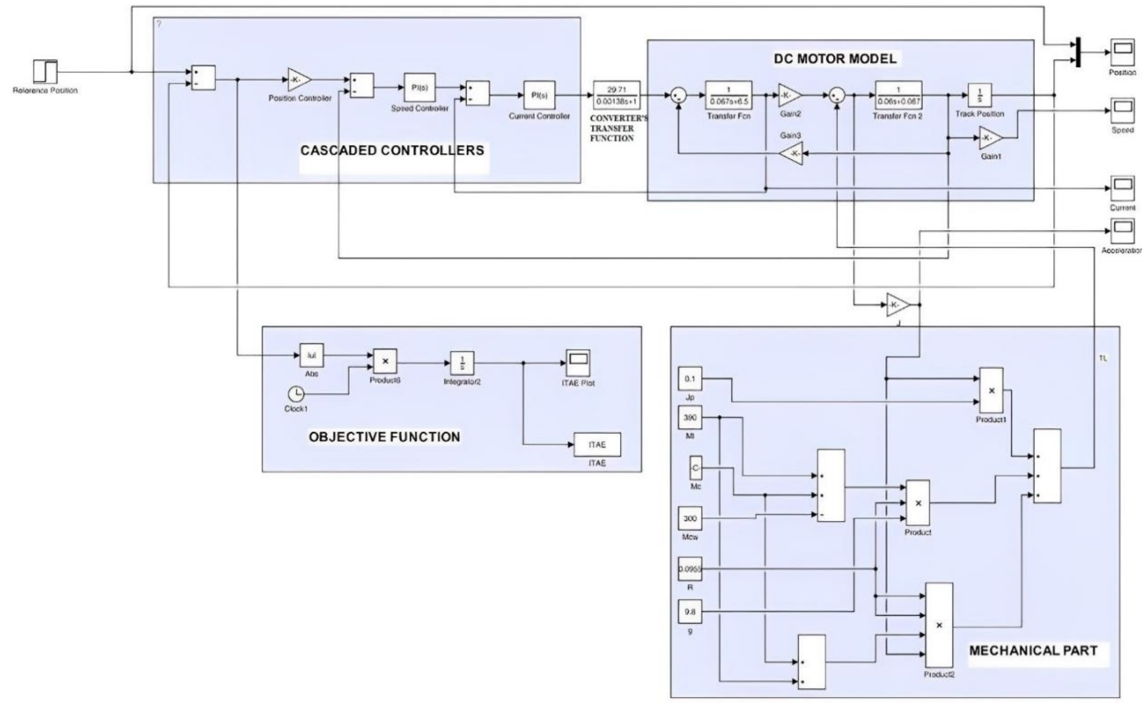

Fig. 11: A simplified circuit diagram of the elevator system with cascaded controllers

Mathematical Modelling of the Mechanical Structures of the Elevator System

Assumptions were made in other to successfully model the elevator's mechanical system. These assumptions are as follows.

The frictional effect from the traveling rope, the governor, and the effect of air pressure on the elevator are neglected.

The suspending pulleys are considered massless from the research (Daka, 2018) Eqs. 60-61 were obtained which described the ascending and descending motion of the elevator's car respectively:

$$\tau_{em} = \left(J_m + \left(M_c + M_l\right)R_p^2 + J_p\right)\frac{d\omega_m}{dt} + b_m\omega_m + \left(M_l + M_c - M_{CW}\right)gR_p \quad (60)$$

$$\tau_{em} = \left(J_m + M_{CW}R_p^2 + J_p\right)\frac{d\omega_m}{dt} + b_m\omega_m + \left(M_{CW} - M_l + M_C\right)gR_p \quad (61)$$

where,
τ_{em} = The electromagnetic torque developed by the motor
J_m = The motor moment of inertia
b_m = The viscous friction coefficient of the motor
ω_m = The angular speed of the motor
M_l = Mass of the load
M_c = Mass of the car
M_{cw} = Mass of the counterweight
V_c = Linear speed of the car
G = Acceleration due to gravity
R_p = Radius of the car pulley

When the elevator's car deaccelerate, the mass of the counterweight is taken into numerical consideration but the mass of the elevator car (M_c) is neglected. (Daka, 2018). Hence during the deceleration of the elevator's car, Eq. 61 becomes approximately equal but opposite in magnitude to Eq. 60. The Eqs. 60-61 were modeled on MATLAB as shown in Fig. 11 to form the mechanical section of the elevator system. The parameters of Table 2 were substituted in the individual blocks forming the mechanical section of the modeled elevator.

Overview of the Integral Time Absolute Error (ITAE)

The objective function block of Fig. 11. received input signals from the error path. The absolute value of the error is multiplied by the simulation time and thereafter integrated to get an accumulated error over time. This error is thereafter sent to the MATLAB workspace (using the ITAE subblock). The ITAE will hub the integration of optimization algorithms into future controller designs for the elevator.

Results and Discussion

The graphical responses of this section were obtained when the modeled elevator was simulated with a reference position command of 100 m. This implied that passengers had the intention of either traveling 100 m above the ground floor of a building utilizing the elevator or descending by 100 m to the ground floor.

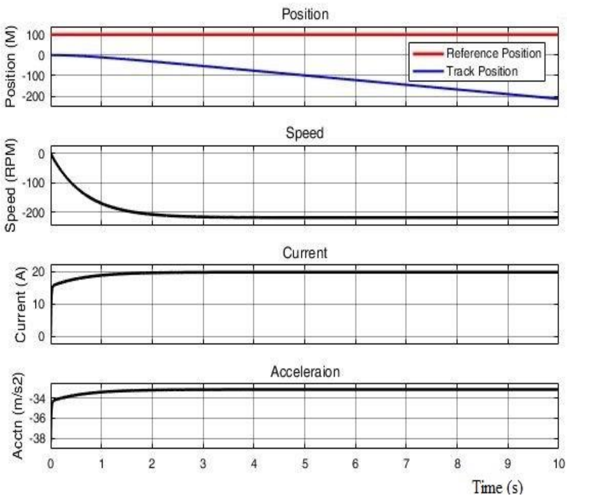

Fig. 12: Ascending responses of the elevator without controllers

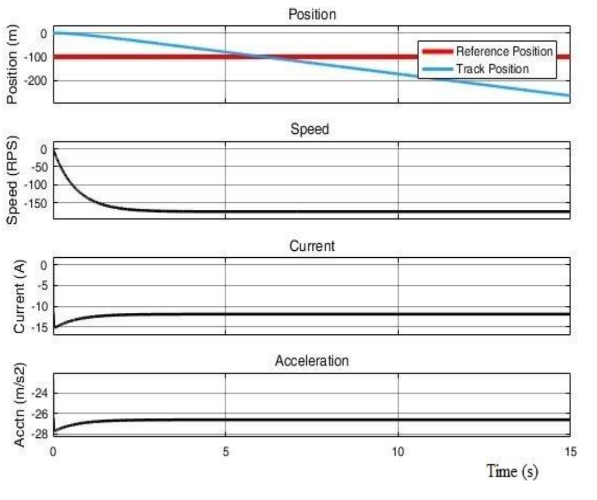

Fig. 13: Descending responses of the elevator without controllers

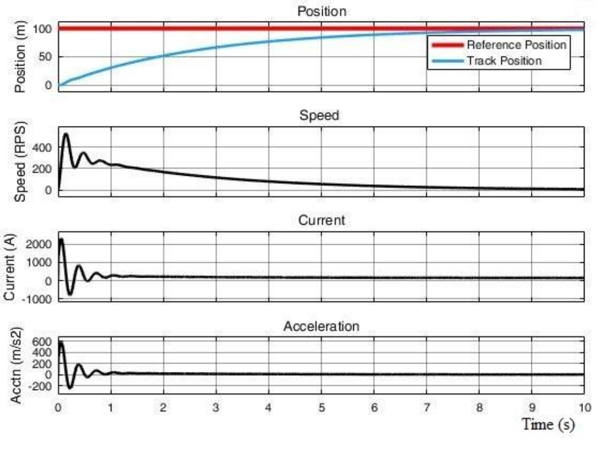

Fig. 14: Ascending responses of the elevator with classically designed controllers

Based on the result obtained from Fig. 12. the position output of the elevator was supposed to track the reference position (since the elevator was ascending to a height of 100 m) and maintain a steady state at that value. However, the elevator never attain a steady state value but diverged from the reference height by decreasing in position. This implied that the elevator system will practically descend when loaded with users whose intention is for the elevator to transport them up to a specified height. It should also be noted that none of the output responses of the elevator reflected the curvature of a second-order control system that the elevator represents.

Considering the speed output response of Fig. 12, it can be inferred that the elevator speed is increasing in the negative direction without settling to zero at a steady state where the maximum height of 100 m was reached. In other words, the motor attained a speed of -200 m/s at a steady state when it was expected to have a speed of zero when reference height was attained. Furthermore, it can be said that the motor was spinning in an anticlockwise direction (negative speed) which was forcing the elevator car to move downwards even when users intended to use the elevator to ascend.

The current output of Fig. 12 (which is proportional to the elevator motor torque) showed that the elevator motor draws a high current of 20 A at a steady state when it was expected to draw a current that was approximately zero. Further inference revealed that the elevator system driven by the motor will continuously run without coming to a halt for passengers to alight when the reference position is reached. This high current of 20 A at a steady state is what is maintaining the elevator speed at -200 m/s at a steady state.

Going on, the acceleration response of Fig. 12. was the derivative of the speed output. At a steady state, the elevator deaccelerates at 34 m/s^2 to maintain a speed of 200 m/s in an anticlockwise direction. It can be concluded from the foregoing that the operation of the elevator is unsatisfactory because of the anticlockwise revolution of the elevator motor when passengers intend to ascend, the divergence of the elevator position from reference, the excessive current drawn, and a settling time of more than one second. These challenges emphasize the need for controllers to be integrated into the elevator system.

The output response of the elevator when descending by 100 m was displayed in Fig. 13. In this regard, the mass of the elevator car (mc) car became neglected during simulation. The descending outputs of the elevator were not satisfactory. The curvature of the position output descended as expected but cut across the reference position without tracking it. The speed output attested that the elevator descended (anticlockwise rotation) but did not achieve an approximately null speed when reference height was achieved. The current drawn by the elevator was lower at a steady state while descending compared to when ascending.

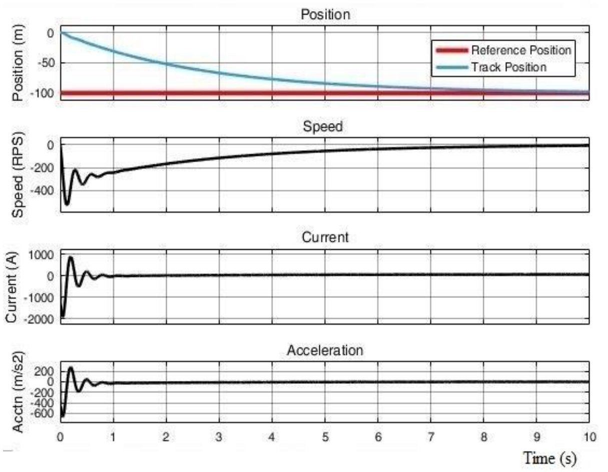

Fig. 15: Descending responses of the elevator with classically designed controllers

This current was measured at 11.5 A at a steady state when it was expected to have a value of almost zero. The current dropped while descending because the mass of the elevator car was negligible.

From Fig. 14 it was inferred that the position response produced the desired curve. However, on zooming out the result, it was found that there was a steady state error of 3.54% which made the settling time of the position output to become infinite. This result which is an improved controller effect may not be suited for an elevator system that requires precision for operation. Further tuning of the controller using algorithms is required to get an updated controller gain for the position controller. The improved gain will be able to annul or mitigate the identified challenges.

For the speed response of Fig. 14, the system was able to also obtain the required curve. However, there were too many damping or oscillations in the system before arriving at a steady state value of 10.45 rad/s. This steady state value is an error because it is desired that at a steady state, the speed of the elevator is zero. Hence, the parameters of the speed controller designed by classical design will introduce an error of 10.45% with an infinite settling time. An improved output will be achieved using tuning algorithms.

For the current response of Fig. 14, there was excessive damping in the system before settling at 5A at an infinite time. Appropriate tuning of the controller gains is required to restore the steady-state current value to at most 0.5A. This current value will keep the elevator ON for the next command by users. The acceleration response curve was desired but the excess damping, overshoot, and settling time of 5 sec will affect the accuracy of the elevator system.

Based on Fig. 15 the descending response of the elevator is opposite of the ascending response of Fig. 14. However, there are two exceptions which are: The acceleration output achieved a steady state at 6 sec which was considered much. Secondly, the current response achieved a steady state response at 1.4 sec but deviated at 2 sec to settle at infinity.

Conclusion

From the result obtained with the classically designed controllers, the errors in the system became mitigated which improved the performance of the entire system. Hence, making linear controllers significant in control systems. Errors were not fully eradicated from the system because of the numerous approximations and assumptions made during the design of the controllers and the modeling of the elevator. However, with the introduction of the objective function block, measured errors will be approximately eradicated with the help of optimization algorithms in future research. Furthermore, irrespective of the position reference chosen, the position output asymptotically tracked its reference while the speed and torque responses at steady state aligned with the curvature of a second-order control system in which the elevator represented bearing approximate errors with the 100m reference. The output responses of the modeled elevator improved the result of reviewed literature based on the asymptotical tracking of the position reference, lesser steady-state errors of the control loops, and the second-order control system curvature of the speed and torque responses at different position references.

Acknowledgment

The research team expresses gratitude to the management of the University of Port Harcourt Rivers State Nigeria, for creating a top-notched environment for research and learning in the Department of Electrical/Electronic Engineering. Special thanks go to the editors and publisher of this article for creating the platform for the research team to share research findings with a wider audience.

Funding Information

The research was unanimously funded by the authors due to the urgent need to solve the observed challenges inhibiting the control of traction elevators and by extension, other DC motors incorporated devices.

Author’s Contributions

Uko Victor Sorochi: Conceived the idea, formulated the mathematical models of the controllers, and supervised the development of the MATLAB Simulink designs.

Kamalu Ugochukwu Anamelechi: Revised the manuscript for clarity and accuracy.

Nwokocha Doris Adaugo: Assisted in the development of the MATLAB schematics and simulations.

Uko Ebenezer Ugochukwu: Wrote the manuscript and analyzed the simulation results.

Ethics

The research is the intellectual property of the authors. It bears their originalities. The research article has not been presented anywhere for publication. Hence, the authors unanimously declare that having perused and approved the manuscript, there will be no forms of ethical issues that may arise after the publication.

References

Adel, Z., Hamou, A. A., & Abdellatif, S. (2018, October). Design of Real-time PID tracking controller using Arduino Mega 2560for a permanent magnet DC motor under real disturbances. In *2018 International Conference on Electrical Sciences and Technologies in Maghreb (CISTEM)* (pp. 1-5). IEEE. https://doi.org/10.1109/CISTEM.2018.8613560

Daka, S. T. (2018). Design and simulation of an elevator DC motor drive with cascade position, speed, and Current Control. Unpublished dissertation in partial fulfillment of the requirements for the degree of Masters of Science, Addis Ababa University. http://bitly.ws/Ru5G

Gücin, T. N., Biberoğlu, M., Fincan, B., & Gülbahçe, M. O. (2015, November). Tuning cascade PI (D) controllers in PMDC motor drives: A performance comparison for different types of tuning methods. In *2015 9th International Conference on Electrical and Electronics Engineering (ELECO)* (pp. 1061-1066). IEEE. https://doi.org/10.1109/ELECO.2015.7394556

Hummadi, R. M. A. M. (2012). Sismulation of optimal speed control for a DC motor using linear quadratic regulator (LQR). *Journal of Engineering*, *18*(03), 340-349. https://search.emarefa.net/detail/BIM-297024

Khan, M. R., Khan, A. A., & Ghazali, U. (2015). Speed control of DC motor under varying load using PID controller. *International Journal of Engineering (IJE)*, *9*(3), 38-48. http://www.cscjournals.org/manuscript/Journals/IJE/Volume9/Issue3/IJE-485.pdf

Pebbles Kids Learning. (2016). *How Do Elevator Work*. [Video file]. Retrieved from. https://www.youtube.com/watch?v=B6usgjKMXz0

Sharkawy, A. N., & Abdel-Jaber, G. T. (2022). Design and Implementation of a Prototype of Elevator Control System: Experimental Work. *SVU-International Journal of Engineering Sciences and Applications*, *3*(2), 80-86. https://doi.org/10.21608/svusrc.2022.149091.1057

Vikhe, P., Punjabi, N., & Kadu, C. (2014). Real time DC motor speed control using PID controller in LabVIEW. *International Journal of Advanced Research in Electrical, Electronics and Instrumentation Engineering*, *3*(9), 12162-12167.

Yang, X., Zhu, Q., & Xu, H. (2008, August). Design and practice of an elevator control system based on PLC. In *2008 Workshop on Power Electronics and Intelligent Transportation System* (pp. 94-99). IEEE. https://doi.org/10.1109/PEITS.2008.44

Yu, J. S., Kim, S. H., Lee, B. K., Won, C. Y., & Hur, J. (2007). Fuzzy-logic-based vector control scheme for permanent-magnet synchronous motors in elevator drive applications. *IEEE Transactions on Industrial Electronics*, *54*(4), 2190-2200. https://doi.org/10.1109/TIE.2007.894692